

Drag Coefficient of a Circular Inclusion in a Near-Critical Binary Fluid Membrane

Hisasi Tani^{1,2*} and Youhei Fujitani^{2†}

¹ *Department of Mechanical Engineering,*

Texas A&M University, TX 77843-3123, USA

² *School of Fundamental Science and Technology,*

Keio University, Yokohama 223-8522, Japan

Abstract

We calculate the drag coefficient of a circular liquid domain, which is put in a flat fluid membrane composed of a binary fluid mixture lying in the homogeneous phase near the demixing critical point. Assuming a sufficiently small correlation length, we regard the domain dynamics as independent of the critical fluctuation and use the Gaussian free-energy functional for the mixture. Because of the near-criticality, the preferential attraction between the domain component and one of the mixture components generates the composition gradient outside the domain significantly and can affect the drag coefficient. We first consider a domain having the same membrane viscosity as the domain exterior. The drag coefficient is expanded with respect to a dimensionless strength of the preferential attraction. It is numerically shown that the magnitude of the expansion coefficient decreases much as the order of the strength increases and that the first-order term of the series usually gives a good approximation for practical material constants. The effect of the preferential attraction is shown to be able to become significantly large in practice. We second consider cases where the membrane viscosities of the domain interior and exterior are different. The first-order term of the expansion series decreases to approach zero as the domain viscosity increases to infinity. This agrees with previous numerical results showing that the hydrodynamics makes the effect of the preferential attraction negligibly small for a rigid disk.

* Email: htani0926@tamu.edu

† Email: youhei@appi.keio.ac.jp

1. INTRODUCTION

A colloidal particle moving translationally with a sufficiently small speed in a quiescent fluid suffers a drag force whose magnitude is proportional to the speed. The constant of the proportionality is called the drag coefficient, and can be related to the self-diffusion coefficient [1–3]. The Brownian motion of a particle gives some informations on the properties of the medium. This kind of probing experiments have been done widely in the microrheology [4, 5], and some have been done for the fluid membrane [6, 7]. The Brownian motion of a trapped particle is now detected with high resolutions of approximately 1 nm and 1 μ s [8, 9].

The drag coefficient of a circular inclusion in a fluid membrane has been studied extensively. A typical example of a fluid membrane is a lipid-bilayer membrane contained in the biomembrane [10, 11]. Regarding a membrane protein as a rigid disk in a flat two-dimensional (2D) fluid immersed in a three-dimensional (3D) fluid, Saffman & Delbrück calculated its drag coefficient by applying the Stokes approximation [12]. The calculation was later performed more thoroughly [13, 14]. The raft hypothesis, which asserts that microdomains enriched in specific lipids, should give platforms to biochemical reactions [15, 16], triggered experimental studies on the phase separation of artificial multicomponent membrane [17–21]. The dispersed phase can take a distinct circular shape, *i.e.*, a circular liquid domain is realized in a fluid membrane. In Koker [22], the drag coefficient of a domain in a flat fluid membrane was calculated on the assumption that the membrane viscosities are the same in the domain interior and exterior. Some researchers measured the diffusion coefficient of a circular liquid domain, and analyzed the results by using the theoretical result for a rigid disk [23] or by assuming that the membrane viscosities are the same in the domain interior and exterior [24]. The drag coefficient of a circular liquid domain with a distinct membrane viscosity in a flat fluid membrane has recently been calculated [25, 26]. Multicomponent membranes near the demixing critical point were also studied experimentally. The observed static critical exponents were found to agree with the ones of the 2D Ising model [27–29], while the observed dynamic critical exponent turned out to be explained in the framework of the model H – a standard model for the near-critical dynamics [30, 31] – with the dynamics in the ambient 3D fluid being taken into account [32–35].

Suppose that a circular inclusion is put in a flat fluid membrane lying in the homogeneous

phase near the demixing critical point [36–38]. Components of the mixture are usually attracted unequally by the inclusion, and thus the composition gradient is generated significantly around the inclusion in the near-critical fluid membrane. An inclusion moving translationally suffers the drag force exerted by the ambient 2D and 3D fluids. Generating the osmotic pressure in the membrane, the composition gradient can alter the flow fields and affect the self-diffusion of the inclusion. However, a previous numerical study on a rigid inclusion showed that the effect is made negligibly small by the hydrodynamics of the ambient 2D and 3D fluids [39]. It thus becomes of interest whether or not the effect remains negligible when the inclusion is a circular liquid domain, considering that its fluidity should alter the ambient flow fields definitely. In this paper, we show that the effect can become significantly large in practice for a circular liquid domain by calculating its drag coefficient.

Our main assumptions are as follows. A flat fluid membrane is immersed in a 3D one-component fluid and contains one circular liquid domain. The membrane outside the domain is a 2D binary fluid mixture lying in the homogeneous phase near the demixing critical point. The other component of the membrane is concentrated in the domain, which is sharply bounded by the mixture. The correlation length of the mixture is much smaller than the domain size. Thus, the domain dynamics can be regarded as independent of the critical concentration fluctuation [40–42], which is remarkable at length scales smaller than the correlation length. The preferential attraction between the domain component and one component of the mixture is caused by a short-ranged interaction. For the mixture, we can apply the hydrodynamics coming from the free-energy functional coarse-grained up to the correlation length. In the experimental results of Honerkamp-Smith *et al.* [27], Veatch *et al.* [28], Honerkamp-Smith *et al.* [29], the 2D mixture is in the critical regime when the correlation length is larger than approximately 100 nm. Thus, the Gaussian free-energy functional, which we use in this study, is expected to be valid when the correlation length is much smaller than 100 nm (and much larger than the microscopic length). In Fujitani [43], one of the present authors studied the drag coefficient of a domain in this situation by assuming that the preferential attraction is sufficiently weak and that the membrane viscosities are the same in the domain interior and exterior. We here calculate the drag coefficient beyond the regime of these assumptions, also correcting errors in Fujitani [43].

Our formulation is shown in Sect. 2. We use the expansion series of the drag coefficient with

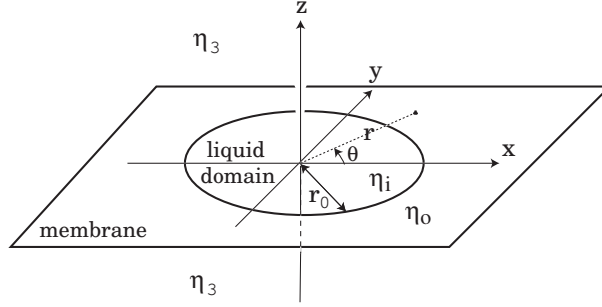


FIG. 1. A circular liquid domain with the radius r_0 in a flat fluid membrane, which stretches infinitely over the xy -plane. The Cartesian coordinate system (x, y, z) and cylindrical coordinate system (r, θ, z) are shown. The membrane viscosities are η_i and η_o inside and outside the domain, respectively, while the viscosity is η_3 in the 3D fluid occupying the semi-infinite spaces on both sides of the membrane.

respect to a dimensionless difference between the membrane viscosities inside and outside the domain and with respect to a dimensionless strength of the preferential attraction. The recurrence relations of the expansion coefficients are derived in Sect. 3, with some details being relegated to Appendix A. The drag coefficient is calculated in Sect. 4, with the numerical procedure being mentioned in Appendix B. Our numerical results are obtained with the aid of Mathematica (Wolfram Research). Some details on the transport coefficients are mentioned in Appendix C, which contains extensions of the results of Inaura and Fujitani [32]. Our results are discussed in Sect. 5.

2. FORMULATION

As shown in Fig. 1, we set the Cartesian coordinate system (x, y, z) and cylindrical coordinate system (r, θ, z) . The flat membrane lies on the xy plane. A circular liquid domain (radius r_0) is fixed with its center being at the origin. The ambient 3D fluid (viscosity η_3) is assumed to occupy the semi-infinite spaces on both sides of the membrane. Imposing a weak homogeneous flow far from the domain, we consider the stationary state and calculate the total force exerted on the fixed domain in the linear regime. The quotient of its magnitude divided by the speed of the homogeneous flow is the drag coefficient γ .

In Sect. 2 A, we assume neither preferential attraction nor near-criticality to review the formulation and procedure in Tani and Fujitani [26], where the membrane outside the domain is regarded

as a 2D one-component fluid. In Sect. 2 B, we mention the points to be altered in the formulation for a near-critical binary fluid membrane. The equations in this subsection are essentially the same as described in Fujitani [43].

A. Case of no preferential attraction

Writing P and \mathbf{V} for the pressure and velocity fields in the 3D fluid, respectively, we have the Stokes equation and the incompressibility condition, *i.e.*,

$$-\nabla P + \eta_3 \Delta \mathbf{V} = 0 \quad \text{and} \quad \nabla \cdot \mathbf{V} = 0 \quad (2.1)$$

for $z \neq 0$. Writing p and \mathbf{v} for these fields in the 2D fluid, we similarly have

$$-\nabla p + \eta \Delta \mathbf{v} + \mathbf{F} = 0 \quad \text{and} \quad \nabla \cdot \mathbf{v} = 0 \quad (2.2)$$

for $r \neq r_0$ and $z = 0$. Here, the differential operator is defined in the two dimensions, the membrane viscosity η equals η_i inside the domain ($r < r_0$) and η_o outside the domain ($r > r_0$), and \mathbf{F} denotes the stress exerted by the 3D fluid lying on both sides of the membrane. Assuming the impermeability of the membrane, we have $V_z \rightarrow 0$ as $z \rightarrow 0$. The no-slip condition gives

$$\lim_{z \rightarrow 0} V_r(r, \theta, z) = v_r(r, \theta) \quad \text{and} \quad \lim_{z \rightarrow 0} V_\theta(r, \theta, z) = v_\theta(r, \theta). \quad (2.3)$$

We write τ for the stress field of the 2D fluid; its rr -component is given by $\tau_{rr} = -p + 2\eta \partial v_r / (\partial r)$. The stress exerted on the domain perimeter in its tangential direction by the domain interior should be balanced with the one by the exterior, and thus we have

$$\lim_{r \rightarrow r_0+} \tau_{r\theta} = \lim_{r \rightarrow r_0-} \tau_{r\theta}, \quad (2.4)$$

where $r \rightarrow r_0 + (-)$ means that r approaches r_0 with $r > r_0$ ($< r_0$) kept. Thus, v_θ is not smooth across $r = r_0$ when η_i is not equal to η_o , as mentioned in Fujitani [25], although V_θ is always smooth in each of the semi-infinite spaces.

The velocity field of the homogeneous flow far from the domain is assumed to be given by $-\varepsilon U e_x$, where e_x is the unit vector along the x -axis, U is a nonzero constant with the dimension of velocity, and ε is a small dimensionless parameter introduced for convenience of later calculations. The total force is along e_x , and its x -component is given by $-\varepsilon \gamma U$ up to the order of ε . Far from

the domain, p and P reach constant values, $p_o^{(0)}$ and $P^{(0)}$, respectively. The velocity fields, \mathbf{V} and \mathbf{v} , are not equal to the homogeneous flow everywhere. We expand the fields with respect to ε . In the 3D fluid, $P^{(1)}$ and $\mathbf{V}^{(1)}$ are so defined that

$$P(\mathbf{r}) = P^{(0)} + \varepsilon P^{(1)}(\mathbf{r}) \quad \text{and} \quad \mathbf{V}(\mathbf{r}) = -\varepsilon U \mathbf{e}_x + \varepsilon \mathbf{V}^{(1)}(\mathbf{r}) \quad (2.5)$$

hold up to the order of ε . Similarly, $p^{(1)}$ and $\mathbf{v}^{(1)}$ are so defined that

$$p(\mathbf{r}) = p^{(0)} + \varepsilon p^{(1)}(\mathbf{r}) \quad \text{and} \quad \mathbf{v}(\mathbf{r}) = -\varepsilon U \mathbf{e}_x + \varepsilon \mathbf{v}^{(1)}(\mathbf{r}) \quad (2.6)$$

hold up to the order of ε . Here, $p^{(0)}$ equals a constant $p_o^{(0)}$ outside the domain and another constant $p_i^{(0)}$ inside the domain. Because the radial component of \mathbf{v} vanishes at the perimeter, we have

$$v_r^{(1)} = U \cos \theta \quad \text{at } r = r_0. \quad (2.7)$$

We also define $\mathbf{F}^{(1)}$ and $\tau^{(1)}$ to have $\mathbf{F} = \varepsilon \mathbf{F}^{(1)}$ and $\tau = \varepsilon \tau^{(1)}$ up to the order of ε . The fields with the superscript $^{(1)}$ vanishes far from the domain.

We introduce the Fourier transforms with respect to θ , *e.g.*,

$$\tilde{V}_{zm}^{(1)}(r, z) \equiv \frac{1}{2\pi} \int_0^{2\pi} d\theta V_z^{(1)}(r, \theta, z) e^{-im\theta}, \quad (2.8)$$

with $m = 0, \pm 1, \pm 2, \dots$. Its Hankel transform is given by

$$\int_0^\infty dr r J_m(\zeta r) \tilde{V}_{zm}^{(1)}(r, z), \quad (2.9)$$

where J_m is the Bessel function of the first kind. Because of the symmetry, the Fourier transforms with $m \neq \pm 1$ vanish. In each field, the transforms of $m = \pm 1$ are related with each other. Thus, we have only to consider the Fourier transforms with $m = 1$. As shown in Appendix A of Tani and Fujitani [26], we rewrite Eq. (2.1) into the Hankel transforms and solve the resultant ordinary differential equations with two functions of ζ being left undetermined. Here, as in Eq. (2.9), ζ is the variable introduced at the Hankel transformation. We can substitute the solution into Eq. (2.2) with the aid of Eq. (2.3) to fix the undetermined functions. As mentioned in Appendix A of Tani and Fujitani [26], we can use the incompressibility conditions to delete one of the two undetermined functions of ζ , and thus have only to consider one undetermined function of ζ . We write $A(\zeta)$ for this function. Introducing

$$\nu_o \equiv \frac{\eta_o}{2\eta_3 r_0} \quad \text{and} \quad J_\pm(\zeta) \equiv J_2(\zeta) \pm J_0(\zeta), \quad (2.10)$$

we obtain

$$\tilde{V}_{r1}^{(1)}(r, z) = \frac{1}{8\eta_3 r_0^2} \int_0^\infty d\zeta \frac{A(\zeta) J_+(\zeta R)}{1 + \nu_o \zeta} e^{-\zeta Z}, \quad (2.11)$$

where R and Z are respectively defined as r/r_0 and z/r_0 ; $i\tilde{V}_{\theta 1}^{(1)}(r, z)$ is given by the above with J_+ being replaced by J_- . The integral above comes from the inverse Hankel transformation. Because $V_z(\mathbf{r})$ vanishes, we have

$$F_r^{(1)} = 2\eta_3 \lim_{z \rightarrow 0+} \frac{\partial V_r^{(1)}}{\partial z} \quad \text{and} \quad F_\theta^{(1)} = 2\eta_3 \lim_{z \rightarrow 0+} \frac{\partial V_\theta^{(1)}}{\partial z}, \quad (2.12)$$

where the factor 2 comes because the force is exerted from both sides of the membrane.

We introduce a dimensionless parameter, defined as

$$\kappa \equiv 1 - \frac{\eta_o}{\eta_i}, \quad (2.13)$$

which vanishes for $\eta_i = \eta_o$. The domain is regarded as a rigid disk when κ approaches unity from below. Extracting the r and θ -components with the order of ε from the first equation of Eq. (2.2), we substitute $\tilde{V}_{r1}^{(1)}$ and $\tilde{V}_{\theta 1}^{(1)}$, which are expressed in terms of A , into the Fourier transforms of the components with the aid of Eq. (2.3). Deleting $\tilde{p}_1^{(1)}$ from the results, we arrive at

$$\int_0^\infty d\zeta \zeta^2 J_1(R\zeta) A(\zeta) = 0 \quad \text{for } R > 1 \quad \text{and} \quad (2.14)$$

$$\int_0^\infty d\zeta \zeta^2 J_1(R\zeta) A(\zeta) \left(1 - \frac{\kappa}{1 + \nu_o \zeta}\right) = 0 \quad \text{for } 0 \leq R < 1, \quad (2.15)$$

which are equivalent to Eqs. (3.5) and (3.6) of Tani and Fujitani [26]. When κ vanishes, *i.e.*, when η_i equals η_o , the left-hand side (lhs) of Eq. (2.15) becomes identical with that of Eq. (2.14).

The x -component of the integral of $\mathbf{F}^{(1)}$ over the domain is given by

$$\int_0^{r_0} dr r \int_0^{2\pi} d\theta \left(F_r^{(1)} \cos \theta - F_\theta^{(1)} \sin \theta \right) = 2\pi \int_0^{r_0} dr r \left(\tilde{F}_{r1}^{(1)} - i\tilde{F}_{\theta 1}^{(1)} \right). \quad (2.16)$$

That of the force exerted on the domain by the membrane outside the domain is given by

$$r_0 \int_0^{2\pi} d\theta \left(\tau_{rr}^{(1)} \cos \theta - \tau_{r\theta}^{(1)} \sin \theta \right) = 2\pi r_0 \left(\tilde{\tau}_{rr1}^{(1)} - i\tilde{\tau}_{r\theta 1}^{(1)} \right), \quad (2.17)$$

which is evaluated in the limit of $r \rightarrow r_0+$. These two equations can be rewritten in terms of $\tilde{V}_{r1}^{(1)}$ and $\tilde{V}_{\theta 1}^{(1)}$ with the aid of Eqs. (2.3) and (2.12)[44]. The sum of Eqs. (2.16) and (2.17) equals $-\gamma U$, and the drag coefficient γ is thus found to be given by [45]

$$\frac{\pi}{r_0 U} \lim_{R \rightarrow 1+} \lim_{Z \rightarrow 0+} \int_0^\infty d\zeta \zeta J_2(\zeta R) A(\zeta) e^{-\zeta Z}. \quad (2.18)$$

The operator Θ is so defined that ΘA denotes the double limits of the integral above. The convergence factor $e^{-\zeta Z}$ is originally contained in $\tilde{V}_{r1}^{(1)}$ and $\tilde{V}_{\theta1}^{(1)}$, as shown in Eq. (2.11). It is later found that $A(\zeta)$ for $\kappa \neq 0$ contains a term proportional to $J_0(\zeta)$, and thus the convergence factor cannot be dropped from Eq. (2.18). Precisely speaking, each integrand of Eqs. (2.14) and (2.15) also has this factor, as mentioned below Eq. (3.24) of Fujitani [25].

We consider the case of $\kappa = 0$ in this paragraph. Because the completeness of the Hankel transformation gives

$$\int_0^\infty d\zeta \zeta J_1(R\zeta) J_1(R'\zeta) = \delta(R - R') , \quad (2.19)$$

we find $A(\zeta) \propto J_1(\zeta)/\zeta$ from Eqs. (2.14) and (2.15) for $\kappa = 0$. The constant of proportionality is fixed by Eq. (2.7), as mentioned in Fujitani [25]. Thus, for $\kappa = 0$, $A(\zeta)$ equals

$$\frac{2\eta_3 r_0^2 U}{\chi} \times \frac{J_1(\zeta)}{\zeta} , \quad (2.20)$$

which satisfies Eq. (2.4) automatically. Here, we use [46]

$$\chi \equiv \int_0^\infty d\zeta \frac{J_1(\zeta)^2}{\zeta^2 (1 + \nu_0 \zeta)} . \quad (2.21)$$

Substituting Eq. (2.20) into Eq. (2.18), we find $\gamma = 2\pi\eta_3 r_0 / \chi$ for $\kappa = 0$, which was first obtained in Koker [22].

Assuming that κ does not always vanish, we introduce

$$\hat{A}(\zeta) \equiv \frac{\chi}{2\eta_3 r_0^2 U} A(\zeta) . \quad (2.22)$$

Noting Eq. (2.20), $\hat{A}(\zeta)$ equals $J_1(\zeta)/\zeta$ when κ vanishes. For this function, we write $\hat{A}_0^{(0)}(\zeta)$, *i.e.*,

$$\hat{A}_0^{(0)}(\zeta) \equiv \frac{J_1(\zeta)}{\zeta} , \quad (2.23)$$

where the subscript $_0$ indicates $\kappa = 0$ and the superscript $^{(0)}$ indicates the absence of the preferential attraction. It is to be noted that the meaning of this superscript is different from the one used in Eqs. (2.5) and (2.6), where the superscript is added to a field. The following procedure applicable for $\kappa \neq 0$ is devised in Fujitani [25] and mentioned more explicitly around Eq. (3.7) of Tani and Fujitani [26]. Irrespective of the value of R , we define $q(R)$ as the integral of Eq. (2.14) with A being replaced by \hat{A} , *i.e.*,

$$q(R) \equiv \int_0^\infty d\zeta \zeta^2 J_1(R\zeta) \hat{A}(\zeta) \quad \text{for } R \geq 0 , \quad (2.24)$$

and then define a finite function $q_1(R)$ to have

$$q(R) = q_1(R) + c_1 \delta(R-1) + c_2 \frac{d}{dR} \delta(R-1) . \quad (2.25)$$

Here, c_1 and c_2 are constants independent of R , and $q_1(R)$ vanishes for $R > 1$ because of Eq. (2.14). The Hankel transformation of Eq. (2.25) involves the integral of $Rq_1(R)J_1(\zeta R)$ over $0 < R < 1$. Rewriting this integral with the aid of Eq. (2.15), we arrive at a single integral equation

$$\hat{A} = \kappa [\mathcal{M}\hat{A}] + (c_1 - \kappa \mathcal{I}\hat{A}) \hat{A}_0^{(0)} - c_2 J_0 , \quad (2.26)$$

where the operators \mathcal{M} and \mathcal{I} are so defined that we have

$$[\mathcal{M}\hat{A}](\xi) = \int_0^\infty d\zeta \frac{\xi J_0(\zeta)J_1(\xi) - \zeta J_0(\xi)J_1(\zeta)}{\xi^2 - \zeta^2} \times \frac{\zeta \hat{A}(\zeta)}{1 + \nu_o \zeta} \quad (2.27)$$

$$\text{and } \mathcal{I}\hat{A} = \int_0^\infty d\zeta \frac{\zeta J_0(\zeta)\hat{A}(\zeta)}{1 + \nu_o \zeta} . \quad (2.28)$$

For $\kappa = 0$, we have $q_1(R) \equiv 0$, $c_1 = 1$, $c_2 = 0$, and Eq. (2.20). For $\kappa \neq 0$, we should fix c_1 and c_2 by using the two conditions of Eqs. (2.4) and (2.7), as described below. In other words, we generally need two constants to fulfill the two conditions.

Let us rewrite the two conditions into convenient forms. With the aid of Eq. (2.3), Eq. (2.11) gives

$$\tilde{v}_{r1}^{(1)}(r) = \frac{U}{2\chi} [\mathcal{L}\hat{A}](R) , \quad (2.29)$$

where the operator \mathcal{L} is so defined that we have

$$[\mathcal{L}\hat{A}](R) = \frac{1}{R} \int_0^\infty d\zeta \frac{J_1(\zeta R)\hat{A}(\zeta)}{\zeta(1 + \nu_o \zeta)} . \quad (2.30)$$

We can rewrite Eq. (2.7) as

$$[\mathcal{L}\hat{A}](1) = \chi , \quad (2.31)$$

into which Eq. (2.26) is substituted to give

$$\kappa [\mathcal{L}\mathcal{M}\hat{A}](1) + (c_1 - \kappa \mathcal{I}\hat{A})\chi - c_2 [\mathcal{L}J_0](1) = \chi . \quad (2.32)$$

In passing, we have Eq. (2.21) because Eq. (2.31) holds even for $\kappa = 0$, and thus $[\mathcal{L}(\hat{A} - \hat{A}_0^{(0)})](1)$ vanishes. With the aid of Eq. (2.3), Eq. (2.11) gives

$$\tilde{\tau}_{r\theta 1} = \frac{-i\eta U}{2r_0\chi} [\mathcal{N}\hat{A}](R) , \quad (2.33)$$

where the operator \mathcal{N} is so defined that we have

$$[\mathcal{N}\hat{A}](R) = \int_0^\infty d\zeta \frac{\zeta J_2'(\zeta R)}{1 + \nu_o \zeta} \hat{A}(\zeta) \quad (2.34)$$

with $J_2'(\zeta)$ denoting $dJ_2(\zeta)/(d\zeta)$. The prime indicates the derivative. As shown by Eq. (3.28) of Fujitani [25], $[\mathcal{N}J_0](R)$ jumps by $1/\nu_o$ as R increases across unity. We define g as $[\mathcal{N}J_0](R)$ in the limit of $R \rightarrow 1+$ [47]. Substituting Eq. (2.26) into Eq. (2.33), we find Eq. (2.4) to give

$$-\kappa^2 [\mathcal{N}\mathcal{M}\hat{A}](1) - \kappa (c_1 - \kappa \mathcal{I}\hat{A}) [\mathcal{N}\hat{A}_0^{(0)}](1) + c_2 \left(\kappa g - \frac{1}{\nu_o} \right) = 0. \quad (2.35)$$

Equations (2.26), (2.32), and (2.35) determine c_1 , c_2 , and \hat{A} , and then γ with the aid of Eqs. (2.18) and (2.22).

B. Near-critical 2D fluid mixture

We here assume that the membrane outside the domain is a 2D binary fluid mixture, as mentioned in the fourth paragraph of Sect. 1. The difference in the mass per unit area between the two components of the mixture can depend on the position \mathbf{r} in the membrane outside the domain. We write $\varphi(\mathbf{r})$ for the difference, which represents the local composition. As in Refs. Okamoto *et al.* [40], Fujitani [43, 48], the φ -dependent part of the free-energy functional is assumed to be

$$\int_{r>r_0} d\mathbf{r} \left(f(\varphi(\mathbf{r})) + \frac{1}{2} M |\nabla \varphi(\mathbf{r})|^2 \right) + r_0 \lim_{r \rightarrow r_0^+} \int_0^{2\pi} d\theta f_s(\varphi(\mathbf{r})). \quad (2.36)$$

The first integral is the area integral over the membrane outside the domain; f is a quadratic function, M is a positive constant, and ∇ represents the two dimensional gradient. The preferential attraction is represented by the second term, which is the line integral over the domain perimeter. The function f_s is here assumed to be a linear function [49]. We write h for the surface field, which is a constant defined as

$$h \equiv -f'_s = -\frac{d}{d\varphi} f_s(\varphi). \quad (2.37)$$

This amounts to considering the dependence of the line tension on φ very near the domain. What is characteristic here is that this dependence causes a significant gradient of φ around the domain in the near-critical 2D fluid. Far from the domain, the mixture is in the homogeneous phase near the demixing critical point. There, φ takes a constant value, for which we write φ_∞ , and the chemical potential conjugate to φ is given by $\mu^{(0)} \equiv f'(\varphi_\infty)$. We thus have

$$f(\varphi) = \frac{m}{2} (\varphi - \varphi_\infty)^2 + \mu^{(0)} (\varphi - \varphi_\infty), \quad (2.38)$$

where m is a positive constant proportional to the temperature measured from the critical one. The correlation length is given by $\sqrt{M/m}$. We define the dimensionless correlation length as

$$s_c \equiv \frac{1}{r_0} \sqrt{\frac{M}{m}}. \quad (2.39)$$

At the equilibrium without the imposed flow, the chemical potential is homogeneously given by $\mu^{(0)}$, and φ minimizes the grand-potential functional coming from Eq. (2.36). The minimization yields

$$\mu^{(0)} = f'(\varphi(\mathbf{r})) - M\Delta\varphi(\mathbf{r}), \quad (2.40)$$

and

$$M\mathbf{e}_r \cdot \nabla\varphi = -h \quad \text{at } r = r_0+, \quad (2.41)$$

where \mathbf{e}_r denotes the radial unit vector. The equilibrium profile of φ depends only on r because of the symmetry, and is thus denoted by $\varphi^{(0)}(r)$, which is given by[43]

$$\varphi^{(0)}(r) = \varphi_\infty + \frac{hr_0s_cK_0(Rs_c^{-1})}{MK_1(s_c^{-1})} \quad \text{for } r > r_0, \quad (2.42)$$

where K_0 and K_1 are modified Bessel functions. The thickness of the adsorption layer, where the preferred component is significantly concentrated, can be regarded as given by the correlation length. For later convenience, we introduce

$$\Phi(R) \equiv \frac{K_1(Rs_c^{-1})}{K_1(s_c^{-1})}, \quad (2.43)$$

which leads to $\varphi^{(0)'}(r) = -h\Phi(R)/M$ for $r > r_0$.

In the stationary state under the imposed flow, $\varphi(\mathbf{r})$ deviates from $\varphi^{(0)}(r)$, and the chemical potential deviates from $\mu^{(0)}$ to become dependent on \mathbf{r} . As discussed in Appendix A of Okamoto *et al.* [40], the chemical potential, denoted by $\mu(\mathbf{r})$, remains given by the right-hand side (rhs) of Eq. (2.40). This can be explained by the local equilibrium, which also makes Eq. (2.41) valid in the dynamics [40, 50, 51]. We assume the transport coefficients outside the domain to be constants independent of the local composition, as in Refs. Camley and Brown [39], Okamoto *et al.* [40], Furukawa *et al.* [41], Fujitani [48]. The diffusive flux between the two components is given by $-L\nabla\mu$, where the Onsager coefficient L is a positive constant. The mass conservation of each component in the stationary state is represented by

$$L\Delta\mu = \mathbf{v} \cdot \nabla\varphi \quad \text{for } r > r_0. \quad (2.44)$$

The diffusive flux does not pass across the perimeter, *i.e.*,

$$\mathbf{e}_r \cdot \nabla \mu = 0 \quad \text{at } r = r_0 + . \quad (2.45)$$

As in Eq. (2.6), $\varphi^{(1)}$ and $\mu^{(1)}$ are so defined that

$$\varphi(\mathbf{r}) = \varphi^{(0)}(r) + \varepsilon \varphi^{(1)}(\mathbf{r}) \text{ and } \mu(\mathbf{r}) = \mu^{(0)} + \varepsilon \mu^{(1)}(\mathbf{r}), \quad (2.46)$$

hold up to the order of ε . The pressure tensor coming from the first term of Eq. (2.36), denoted by Π , is used in the model H [30, 31]. We have

$$\Pi = \left(-f + \mu\varphi - \frac{M}{2} |\nabla \varphi|^2 \right) \mathbf{1} + M \nabla \varphi \nabla \varphi, \quad (2.47)$$

where $\mathbf{1}$ denotes the isotropic tensor. The osmotic pressure, $\varphi f' - f$, is thus contained in Eq. (2.47). The term, $-\nabla \cdot \Pi = -\varphi \nabla \mu$ should be added to the lhs of the first equation of Eq. (2.2) for $r > r_0$. Accordingly, Eq. (2.14) is replaced by

$$\int_0^\infty d\zeta \, \zeta^2 J_1(R\zeta) A(\zeta) = \frac{2r_0^3 \varphi^{(0)'}(r) \tilde{\mu}_1^{(1)}(r)}{R} \quad \text{for } R > 1, \quad (2.48)$$

while Eq. (2.15) is unchanged. We here introduce a dimensionless surface field

$$\lambda \equiv \frac{hr_0}{M} \sqrt{\frac{r_0}{2\eta_3 L}}. \quad (2.49)$$

Picking up the terms with the order of ε from Eq. (2.44) and solving the resultant equation formally, we can express $\tilde{\mu}_1^{(1)}$ in terms of Eq. (2.29), as shown in Appendix A. As a result, we can rewrite Eq. (2.48) as

$$\int_0^\infty d\zeta \, \zeta^2 J_1(R\zeta) \hat{A}(\zeta) = \lambda^2 \frac{\Phi(R)}{R} \left[\Delta_1^{-1} \Phi(\mathcal{L}\hat{A} - \chi) \right](R) \quad \text{for } R > 1. \quad (2.50)$$

Here, the operator Δ_1^{-1} is so defined that a function Ω is transformed into

$$\left[\Delta_1^{-1} \Omega \right](R) = \int_1^\infty dR' \, \frac{G(R, R')}{R} \Omega(R'), \quad (2.51)$$

where the kernel $G(R, R')$ is defined as $-(1 + R'^2)/2$ for $R' \leq R$ and as $-(1 + R^2)/2$ for $1 < R < R'$.

From Eqs. (2.15) and (2.50), we can obtain a single integral equation in the presence of the preferential attraction in the near-criticality by using essentially the same procedure as mentioned in Sect. 2 A. Here, for $R > 1$, $q_1(R)$ of Eq. (2.25) does not vanish but equals the rhs of Eq. (2.50). Accordingly, the term

$$\lambda^2 \left[\mathcal{H} \Delta_1^{-1} \Phi(\mathcal{L}\hat{A} - \chi) \right](\zeta) \quad (2.52)$$

is added on the rhs of Eq. (2.26). Here, the operator \mathcal{H} is so defined that a function Ω is transformed into

$$[\mathcal{H}\Omega](\zeta) = \frac{1}{\zeta} \int_1^\infty dR \Phi(R) J_1(\zeta R) \Omega(R). \quad (2.53)$$

Equation (2.4) remains valid in the presence of the preferential attraction because the free-energy functional given by Eq. (2.36) does not contribute to the tangential stress exerted on the domain [43]. The same situation for a 3D droplet is discussed in Appendix D of Fujitani [52]. Equation (2.7) also remains available here. Thus, as in Sect. 2 A, we can use Eqs. (2.4) and (2.7) to fix c_1 and c_2 , which are contained in Eq. (2.26) supplemented with Eq. (2.52).

In the presence of the preferential attraction, as in its absence, \mathbf{F} and τ still contribute to the drag force. In calculating the latter contribution, we should note that the term $-\varphi \nabla \mu$ is added to the lhs of the first equation of Eq. (2.2). Furthermore, the drag force has a contribution from Π , *i.e.*, should have a term of

$$-r_0 \lim_{r \rightarrow r_0^+} \int_0^{2\pi} d\theta \Pi \cdot \mathbf{e}_r. \quad (2.54)$$

The contribution from the second term of Eq. (2.36) vanishes. Summing up all these contributions, we find that γ is given by the sum of Eq. (2.18) and

$$\frac{2\pi\eta_3 r_0 \lambda^2}{\chi} \int_1^\infty dR R \Phi(R) \left[\Delta_1^{-1} \Phi(\mathcal{L}\hat{A} - \chi) \right](R). \quad (2.55)$$

See Appendix A for some details.

3. RECURRENCE RELATIONS

We expand \hat{A} with respect to κ as

$$\hat{A}(\zeta) = \sum_{n=0}^{\infty} \hat{A}_n(\zeta) \kappa^n, \quad (3.1)$$

whereby $\hat{A}_n(\zeta)$ is defined. Similarly, we expand c_1 and c_2 as

$$c_1 = \sum_{n=0}^{\infty} \alpha_n^\# \kappa^n \quad \text{and} \quad c_2 = - \sum_{n=0}^{\infty} \beta_n \kappa^n, \quad (3.2)$$

where $\alpha_n^\#$ and β_n are the expansion coefficients independent of κ . Then, we define α_n as $\alpha_n^\# - \mathcal{I}\hat{A}_{n-1}$ for $n \geq 1$ with α_0 being put equal to $\alpha_0^\#$. The dynamics is invariant against the exchange of the

components in the 2D mixture, and thus against the change of the sign of h . Thus, we can expand \hat{A}_n , α_n , and β_n with respect to λ^2 , which represents the strength of the preferential attraction, as

$$\hat{A}_n = \sum_{k=0}^{\infty} \hat{A}_n^{(k)} \lambda^{2k}, \quad \alpha_n = \sum_{k=0}^{\infty} \alpha_n^{(k)} \lambda^{2k}, \quad \text{and} \quad \beta_n = \sum_{k=0}^{\infty} \beta_n^{(k)} \lambda^{2k}, \quad (3.3)$$

whereby $\hat{A}_n^{(k)}$, $\alpha_n^{(k)}$, and $\beta_n^{(k)}$ are defined. We similarly expand the drag coefficient as

$$\gamma = \frac{2\pi\eta_3 r_0}{\chi} \left(\sum_{n=0}^{\infty} \hat{\gamma}_n \kappa^n \right) \quad \text{and} \quad \hat{\gamma}_n = \sum_{k=0}^{\infty} \hat{\gamma}_n^{(k)} \lambda^{2k}. \quad (3.4)$$

The expansion coefficients, $\hat{\gamma}_n$ and $\hat{\gamma}_n^{(k)}$, are here introduced. We have $\hat{\gamma}_0^{(0)} = 1$ because of the statement below Eq. (2.21). The sum in the parentheses of the first entry of Eq. (3.4) gives the ratio of γ to its value for $\kappa = \lambda = 0$ and is below referred to as dimensionless drag coefficient, for which we write $\hat{\gamma}$. From Eqs. (2.18) and (2.55), we find

$$\hat{\gamma} = \Theta \hat{A} + \lambda^2 \int_1^{\infty} dR R \Phi(R) \left[\Delta_1^{-1} \Phi(\mathcal{L} \hat{A} - \chi) \right] (R), \quad (3.5)$$

where the operator Θ is defined below Eq. (2.18).

A. Terms studied previously

The terms with $k = 0$ in Eqs. (3.3) and (3.4) are calculated in Tani and Fujitani [26], where the drag coefficient is studied in the absence of the preferential attraction, *i.e.*, for $\lambda = 0$. For convenience of later description, we here review their recurrence relations. Substituting Eqs. (3.1) and (3.2) into Eqs. (2.26), (2.32), and (2.35), we find $\alpha_0^{(0)} = 1$, $\beta_0^{(0)} = 0$, $\hat{A}_0^{(0)}(\zeta) = J_1(\zeta)/\zeta$,

$$\beta_n^{(0)} = \nu_0 \left(\alpha_{n-1}^{(0)} \left[\mathcal{N} \hat{A}_0^{(0)} \right] (1) + \beta_{n-1}^{(0)} g + \left[\mathcal{N} \mathcal{M} \hat{A}_{n-2}^{(0)} \right] (1) \right), \quad (3.6)$$

$$\alpha_n^{(0)} = -\frac{1}{\chi} \left(\beta_n^{(0)} \left[\mathcal{L} J_0 \right] (1) + \left[\mathcal{L} \mathcal{M} \hat{A}_{n-1}^{(0)} \right] (1) \right), \quad (3.7)$$

$$\text{and} \quad \hat{A}_n^{(0)} = \alpha_n^{(0)} \hat{A}_0^{(0)} + \beta_n^{(0)} J_0 + \left[\mathcal{M} \hat{A}_{n-1}^{(0)} \right] \quad (3.8)$$

for $n = 1, 2, \dots$, where we stipulate $\hat{A}_{-1}^{(0)} \equiv 0$. Putting λ equal to zero in Eq. (3.4), we find the dimensionless drag coefficient to be given by

$$\hat{\gamma} = 1 + \sum_{n=1}^{\infty} \hat{\gamma}_n^{(0)} \kappa^n \quad \text{for } \lambda = 0. \quad (3.9)$$

For convenience of numerical calculations, we utilize Eq. (3.8) in Eq. (3.5) to obtain

$$\hat{\gamma}_n^{(0)} = \alpha_n^{(0)} + 2\beta_n^{(0)} + \Theta \mathcal{M} \hat{A}_{n-1}^{(0)} \quad \text{for } n = 0, 1, 2, \dots \quad (3.10)$$

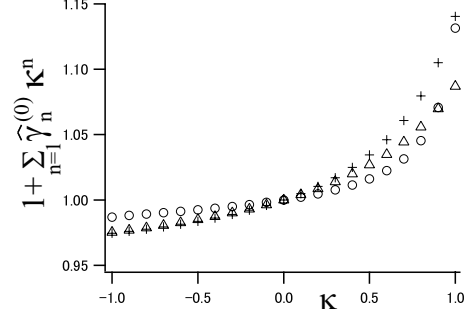


FIG. 2. Plot of Eq. (3.9) against κ , which is a replot of the results in Tani and Fujitani [26]. Circles, crosses, and triangles represent the results for $\nu_0 = 0.1, 1$, and 10 . For these values, we calculate Eq. (3.9) by truncating the series appropriately, *i.e.*, up to $n = 35, 15$, and 10 , respectively, as in Tani and Fujitani [26].

With the aid of numerical integrations, Eq. (3.9) is calculated for $-1 < \kappa < 1$ and some values of ν_0 in Tani and Fujitani [26], where the calculation results in the limit of $\kappa \rightarrow 1-$ are shown to agree with the results for a rigid disk in Saffman & Delbrück's model [12–14]. Figure 2 shows numerical results of Eq. (3.9), which gives the ratio of γ for $\lambda = 0$ to its value for $\kappa = \lambda = 0$. As mentioned in Tani and Fujitani [26], it is hard to calculate Eq. (3.9) numerically for $\kappa < -1$.

B. Higher-order terms with respect to λ^2

In the presence of the preferential attraction in the near-criticality, substituting Eq. (2.26) supplemented with Eq. (2.52) into Eq. (2.31) yields Eq. (2.32) supplemented with

$$\lambda^2 \left[\mathcal{LH}\Delta_1^{-1}\Phi \left(\mathcal{L}\hat{A} - \chi \right) \right] (1) \quad (3.11)$$

on the lhs. Noting that $\left[\mathcal{NH}\Delta_1^{-1}\Phi \left(\mathcal{L}\hat{A} - \chi \right) \right] (R)$ is continuous at $R = 1$, we similarly find that the term

$$-\kappa\lambda^2 \left[\mathcal{NH}\Delta_1^{-1}\Phi \left(\mathcal{L}\hat{A} - \chi \right) \right] (1) \quad (3.12)$$

is supplemented on the lhs of Eq. (2.35). We use these supplementations to modify the recurrence relations Eqs. (3.6)-(3.8), as mentioned in Appendix A, where we also modify Eq. (3.10) by using Eq. (3.5). Each of $\hat{\gamma}_n^{(1)}, \hat{\gamma}_n^{(2)}, \dots$ depends on ν_0 and s_c .

$\hat{\gamma}_n^{(k)}$	$k=0,$	<div style="display: flex; justify-content: space-around; align-items: center;"> <div style="border: 1px solid black; padding: 5px; text-align: center;">Sect. 4.1</div> <div style="border: 1px solid black; padding: 5px; text-align: center;">Sect. 4.2</div> </div>		<div style="display: flex; align-items: center;"> <div style="border-left: 1px solid black; border-right: 1px solid black; padding: 0 5px;">Sect. 3.1</div> <div style="border-left: 1px solid black; padding: 0 5px;">Sect. 3.2</div> </div>
	$n=0, 1, 2, 3, \dots$	de Koker (1996)	Tani & Fujitani (2018)	

FIG. 3. The values of (n, k) for $\hat{\gamma}_n^{(k)}$ discussed in each subsection are shown. In the absence of the preferential attraction ($\lambda = 0$), de Koker [22] found that γ for $\kappa = 0$ is given by $2\pi\eta_3 r_0/\chi$. Dividing γ by de Koker's result, we consider the series expansion of the quotient with respect to κ and λ^2 , as shown by Eq. (3.4); $\hat{\gamma}_0^{(0)}$ equals unity. The series for $\lambda = 0$ is given by Eq. (3.9) and was studied by Tani & Fujitani [26], as described in Sect. 3 A. The series in the presence of the preferential attraction is mentioned in Sect. 3 B. We show the results of $\hat{\gamma}_0^{(1)}, \hat{\gamma}_0^{(2)}, \hat{\gamma}_0^{(3)}, \dots$ in Sect. 4 A, and those of $\hat{\gamma}_0^{(1)}, \hat{\gamma}_1^{(1)}, \hat{\gamma}_2^{(1)}, \dots$ in Sect. 4 B.

4. RESULTS

In the presence of the preferential attraction in the near-criticality, we study the drag coefficient of a domain with $\eta_i = \eta_o$ in Sect. 4 A, and study how the drag coefficient changes with $\kappa \equiv 1 - (\eta_o/\eta_i)$ in Sect. 4 B. What coefficients in the second series of Eq. (3.4) are discussed in each subsection is summarized in Fig. 3. The recurrence relations shown in Sect. 3 B and the following results are newly obtained in the present study. Errors in Fujitani [43], where only $\hat{\gamma}_0^{(1)}$ was studied, are pointed out in Appendix A.

A. Results for $\kappa = 0$

Putting κ equal to zero in Eq. (3.4), we find the dimensionless drag coefficient to be given by

$$\hat{\gamma} = \hat{\gamma}_0 = 1 + \sum_{k=1}^{\infty} \hat{\gamma}_0^{(k)} \lambda^{2k} \quad \text{for } \kappa = 0. \quad (4.1)$$

The second term on the rhs above represents the ratio of the deviation of γ from de Koker's result[22] – the drag coefficient with $\eta_i = \eta_o$ in the absence of the preferential attraction. We can calculate $\hat{\gamma}_0^{(1)}, \hat{\gamma}_0^{(2)}, \dots$ by putting n to be equal zero in the recurrence relations mentioned in

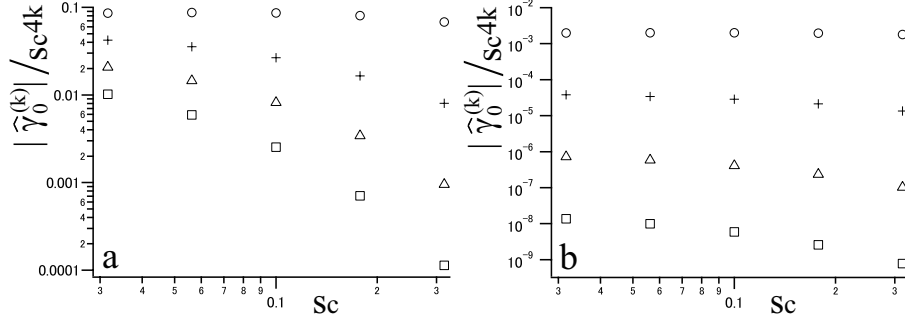


FIG. 4. Plots of $|\hat{\gamma}_0^{(k)}|/s_c^{4k}$ against s_c for $\nu_o = 0.1$ (a) and 10 (b). Circles, crosses, triangles, and squares represent the values for $k = 1, 2, 3$, and 4, respectively.

Sect. 3 B, *i.e.*, Eqs. (A.12)-(A.15), where some terms vanish because of $\beta_0^{(k)} = A_{-1}^{(k)} = 0$. The initial terms $\alpha_0^{(0)}$ and $\hat{A}_0^{(0)}$ are mentioned in Sect. 3 A. Our numerical procedure for calculating the integrals contained in the expansion coefficients is described in Appendix B. To show their dependence on ν_o and s_c , we plot the ratio $|\hat{\gamma}_0^{(k)}|/s_c^{4k}$ against s_c for $k = 1, \dots, 4$ in Fig. 4. The results of $\hat{\gamma}_0^{(1)}$ and $\hat{\gamma}_0^{(3)}$ are positive, while those of $\hat{\gamma}_0^{(2)}$ and $\hat{\gamma}_0^{(4)}$ are negative. In Fig. 4, $|\hat{\gamma}_0^{(k)}|$ is smaller than a constant multiplied by s_c^{4k} , which suggests that Eq. (4.1) converges at least when $\lambda^2 s_c^4$ is smaller than unity. As expected, the series appears to converge even for sufficiently large values of λ^2 in Fig. 5, where $\hat{\gamma}_0^{(k)}$ is positive for $k = 1, 3, 5, \dots$ and negative for $k = 2, 4, 6, \dots$. For $\lambda^2 = 5000$ in this figure, the results appears independent of K and thus $1 + \hat{\gamma}_0^{(1)}\lambda^2$ is suggested to give a good approximation to Eq. (4.1). It is suggested to give a rather good approximation for $\lambda^2 = 10^4$. For larger λ^2 , some higher-order terms would be required for estimating the sum to the second decimal place. In our numerical results not shown here, Eq. (4.1) for $(\nu_o, s_c) = (1, 0.1)$ appears to converge even when λ^2 is raised up to 10^5 approximately; the upper bound of λ^2 for the convergence increases as ν_o increases. This can be expected from Fig. 4; $\hat{\gamma}_0^{(k)}$ for the larger value of ν_o decreases more rapidly as k increases. In Fig. 4, $|\hat{\gamma}_0^{(k)}|$ for a given set of k and s_c is smaller for the larger value of ν_o , and $|\hat{\gamma}_0^{(k)}|$ increases with s_c for a given set of k and ν_o . Thus, $|\hat{\gamma}_0^{(k)}|$ would increase as s_c increases and as ν_o decreases.

The Onsager coefficient L of Eq. (2.44) depends on the correlation length because of the critical fluctuation, as mentioned in Appendix C. The dependence of η_o on the correlation length is there shown to be very weak and is here neglected. Noting Eq. (C.3) and the statement above it, we

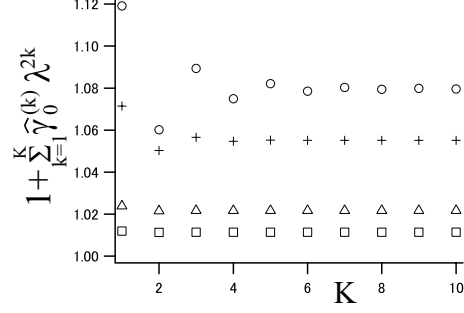


FIG. 5. Plot of the sum of $\hat{\gamma}_0^{(k)} \lambda^{2k}$ from $k = 0$ to K against K for $\nu_o = 1$ and $s_c = 0.1$. We use $\lambda^2 = 50000$ (circles), 30000 (crosses), 10000 (triangles), and 5000 (squares).

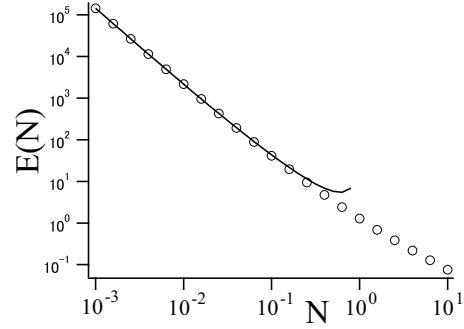


FIG. 6. Plot of $E(N)$ against N (circles). The solid curve drawn for $N < 1$ represents $-1/N^2 / \ln N$.

rewrite L in Eq. (2.49) to obtain

$$\lambda^2 \approx \frac{4\pi h^2 r_0^2}{M\nu_o k_B T} E(N), \quad (4.2)$$

where k_B is the Boltzmann constant, T is the temperature, N is defined as s_c/ν_o , and E is a function defined as

$$E(N) \equiv \frac{2(1 + N^2)}{N^2(\pi N - 2 \ln N)}. \quad (4.3)$$

In Fig. 6, $E(N)$ decreases as N increases and $E(N)$ is approximated to be $-1/N^2 / \ln N$ for $N \ll 1$. We can also find from this figure that $NE(N)$ decreases as N increases. Thus, λ^2 increases as ν_o increases and as s_c decreases.

As mentioned in Fujitani [53], when a wall is in contact with a 3D near-critical binary fluid mixture, a typical value of the surface field is $10^{-7} \text{ m}^3/\text{s}^2$ on the basis of the discussion in Liu and Fisher [54], while one of the coefficient of the square gradient term in the free-energy functional

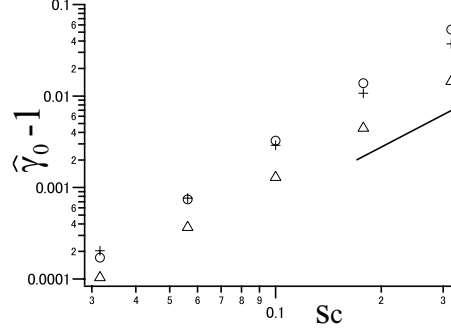


FIG. 7. Plots of $\hat{\gamma}_0 - 1$ against s_c for $\nu_o = 0.1$ (circles), 1 (crosses), and 10 (triangles). We calculate the second term on the rhs of Eq. (4.1) by truncating the series up to $k = 10$. The values of λ^2 are obtained from Eq. (4.2) and the parameter values mentioned in the text. They are respectively 10^3 multiplied by 2.0, 0.86, 0.38, 0.18, and 0.086 for the circles from the extreme left to the right, 10^3 multiplied by 8.6, 3.2, 1.2, 0.49, and 0.20 for the crosses, and 10^3 multiplied by 52, 18, 6.5, 2.3, and 0.86 for the triangles. The solid line with the slope of two is drawn for a guide of view.

is $10^{-16} \text{ m}^7/(\text{s}^2 \cdot \text{kg})$ [55, 56]. We use the former value for h in the membrane, and divide the latter value by a typical membrane thickness, *i.e.*, several nanometers, to use the quotient for M in the membrane, *i.e.*, to use $M = 10^{-8} \text{ m}^6/(\text{s}^2 \cdot \text{kg})$. We assume $r_0 = 100 \text{ nm}$; typical values of $\eta_o \approx 10^{-7} \text{ dyn} \cdot \text{s}/\text{cm}$ [57] and $\eta_3 \approx 10^{-2} \text{ dyn} \cdot \text{s}/\text{cm}^2$ yield $\nu_o \approx 1$. Assuming $T = 300 \text{ K}$, we find the fraction in Eq. (4.2) to be 30 approximately. We also study cases of $\nu_o = 0.1$ and 10, for which the values of the fraction are put equal to 300 and 3, respectively. For these parameter values, we numerically calculate the ratio of the deviation due to the preferential attraction, which is given by the second term on the rhs of Eq. (4.1), by truncating the series up to $k = 10$, and plot the results in Fig. 7. As mentioned below, we can obtain almost the same figure by using only the term with $k = 1$ in the series. The difference between the single term $\hat{\gamma}_0^{(1)} \lambda^2$ and the sum of the 10 terms increases as s_c increases and as ν_o decreases, but rather insensitive to ν_o . The differences at $\nu_o = 0.1$ are respectively 4×10^{-5} , 5×10^{-4} , and 5×10^{-3} for $s_c = 0.1$, 0.18, and 0.32. They are respectively much smaller than the corresponding results in Fig. 7.

In Fig. 7, the ratio of the deviation due to the preferential attraction increases with s_c and is roughly proportional to s_c^2 ; the ratio reaches several percent for $\nu_o = 0.1$ and 1. The increase with s_c is reasonable, considering that the adsorption layer becomes thicker with s_c . As mentioned

above, the increase of $\hat{\gamma}_0^{(1)}$ and the decrease of λ^2 occur when s_c increases and when ν_o decreases. The increase of the deviation ratio with s_c shown in Fig. 7 represents the predominance of the effect of the increase of $\hat{\gamma}_0^{(1)}$ over that of the decrease of λ^2 . This predominance can also explain that the deviation ratio for a given s_c is the smallest for $\nu_o = 10$. For larger ν_o , effects of the viscous stress in the 2D mixture increases and the relative contribution from Π to the drag force would decrease. However, the deviation ratio is not so much different for $\nu_o = 1$ and 0.1 in Fig. 7, which suggests that the effects of $\hat{\gamma}_0^{(1)}$ and λ^2 are balanced with each other. As described in the caption of Fig. 7, λ^2 is approximately 1200 for $\nu_o = 1$ and $s_c = 0.1$. If h doubles and M halves from their respective estimates mentioned above, λ^2 increases up to 10^4 approximately because of Eq. (4.2). Then, the deviation ratio becomes approximately 2 % in Fig. 5, where the ratio is found to reach several percent when λ^2 doubles or triples further.

B. Results up to the order of λ^2

Because of Eq. (3.4), we have

$$\hat{\gamma} = 1 + \sum_{n=1}^{\infty} \hat{\gamma}_n^{(0)} \kappa^n + \lambda^2 \sum_{n=0}^{\infty} \hat{\gamma}_n^{(1)} \kappa^n \quad (4.4)$$

up to the order of λ^2 . The sum of the first two terms on the rhs above is calculated in Sect. 3 A. Here, we numerically calculate $\hat{\gamma}_n^{(1)}$ by using Eqs. (A.11)-(A.15). In Fig. 8(a), $\hat{\gamma}_0^{(1)}$ is positive, while some of the subsequent terms, such as $\hat{\gamma}_1^{(1)}$, $\hat{\gamma}_2^{(1)}$, and $\hat{\gamma}_3^{(1)}$, are negative. In Fig. 8(b), the third term on the rhs of Eq. (4.4) decreases as κ increases from -1 to 1 . As κ approaches unity, the third term becomes close to zero, which means that the sum of the negative terms then almost cancel out the positive term. The positivity of $\hat{\gamma}_0^{(1)}$ comes from the term involving χ in Eq. (3.5), and this term does not appear explicitly in the expression of $\hat{\gamma}_n^{(k)}$ for $(n, k) \neq (0, 1)$, as mentioned at the end of Appendix A. In passing, the result for $\kappa = 0$ in Fig. 8(b) is given by $\lambda^2 \hat{\gamma}_0^{(1)}$ and agrees well with the value shown by the cross for $s_c = 0.1$ in Fig. 7, as expected from the results of Fig. 5.

The ratio of the deviation due to the preferential attraction is given by the quotient of the third term divided by the sum of the first two terms on the rhs of Eq. (4.4). For $s_c = 0.1$ and some values of ν_o , we numerically calculate this deviation ratio and plot the results in Fig. 9. The ratio for each of the values of ν_o monotonically decreases to approach zero as κ increases to unity, like the results in Fig. 8(b). We find that the results for $s_c = 0.1$ in Fig. 7 respectively agree well with

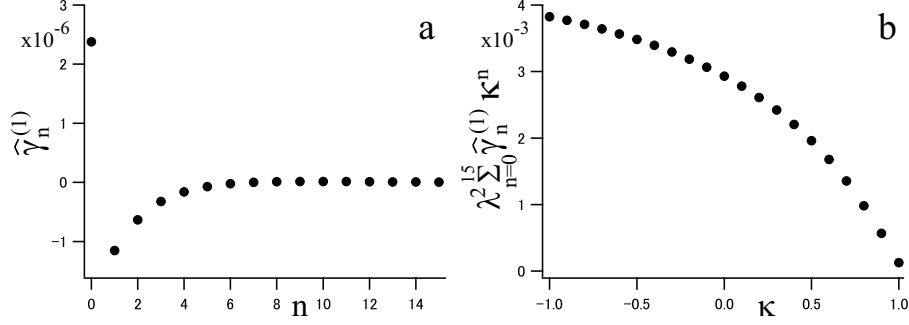


FIG. 8. Results for $\nu_o = 1$ and $s_c = 0.1$. (a) Plot of $\hat{\gamma}_n^{(1)}$ against n . (b) Plot of the third term on the rhs of Eq. (4.4) against κ . Numerically, we truncate the series given by the third term up to $n = 15$, like the corresponding series used in Fig. 2. We use $\lambda^2 = 1.2 \times 10^3$, which is the same as used for $\nu_o = 1$ and $s_c = 0.1$ in Fig. 7.

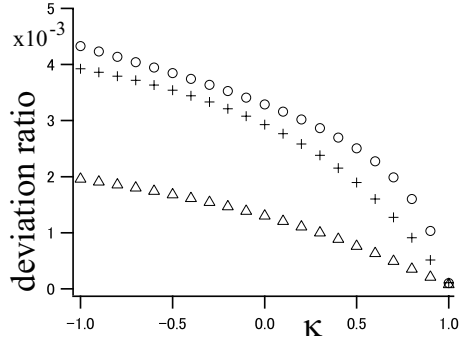


FIG. 9. Plot of the ratio of the third term to the sum of the first two terms on the rhs of Eq. (4.4) against κ for $s_c = 0.1$. Circles, crosses, and triangles represent the results for $\nu_o = 0.1, 1$, and 10 , respectively. Numerically, for each value of ν_o , the two series in Eq. (4.4) are truncated in the same way as used in Fig. 2. For these values of ν_o , as in Fig. 7, we respectively use $\lambda^2 = 3.8 \times 10^2, 1.2 \times 10^3$, and 6.5×10^3 .

the corresponding results for $\kappa = 0$ in Fig. 9. This means that, for the parameter values used in this figure, $\hat{\gamma}$ is well given by Eq. (4.4) when κ vanishes.

5. DISCUSSION

We consider a circular liquid domain, which is put in a flat fluid membrane composed of a binary fluid mixture lying in the homogeneous phase near the demixing critical point. The corre-

lation length is assumed to be much smaller than the domain size. The domain dynamics is thus regarded as independent of the critical fluctuation, which is significant at length scales smaller than the correlation length and makes the Onsager coefficient dependent on the correlation length. Because of the near-criticality, the preferential attraction between the domain component and one of the component of the mixture generates the composition gradient outside the domain significantly and can affect the drag coefficient. The correlation length is also assumed to be so small as to validate the Gaussian model.

In Sect. 4 A, we calculate the dimensionless drag coefficient for $\kappa = 0$, *i.e.*, for a domain with $\eta_i = \eta_o$. There, the expansion series with respect to λ^2 , which represents the strength of the preferential attraction, is found to be helpful even for large values of λ^2 because the expansion coefficient decreases much as the order of λ^2 increases. We can obtain a good approximation to the second term on the rhs of Eq. (4.1) by calculating only the first term of the series for practical values of λ^2 . As shown in Fig. 7, the deviation of the drag coefficient for $\kappa = 0$ due to the preferential attraction increases with the correlation length and can reach several percent of the one in the absence of the preferential attraction for some practical material constants. Dependence of the deviation on the correlation length is steeper than linear. The drag coefficient for $\kappa = \lambda = 0$ was obtained in Koker [22] and is given below Eq. (2.21); its dependence on r_0 is not steeper than linear, as shown in Fig. 4 of Fujitani [58]. Thus, the dependence of the deviation cannot be explained naively by effective enlargement of the domain radius due to the adsorption layer, whose thickness can be regarded as the correlation length.

In Sect. 4 B, we calculate the dimensionless drag coefficient up to the order of λ^2 , not assuming $\kappa = 0$. In Fig. 9, the effect of the preferential attraction decreases as κ increases from -1 to 1 and becomes negligibly small for a rigid disk. The truncation up to the order of λ^2 gives a good approximation for the parameter values used in this figure when κ vanishes. We expect that it remains the case for $\kappa \neq 0$, considering that, as far as examined, the magnitudes of the expansion coefficients are correlated with each other through the recurrence relations. Our results qualitatively agree with one of the results of Camley and Brown [39] showing that the effect on a rigid disk should be negligibly small. The results were obtained with the aid of the immersed boundary method[59], where the boundary condition at the perimeter is altered from the no-slip condition. In this previous study, it was also claimed that the hydrodynamics reduces the effect

on a rigid disk. This is also consistent with our results showing that the effect becomes larger for a less viscous liquid domain, whose fluidity should alter the flow fields more definitely from the one around a rigid disk with the same size.

For detecting the effect of the preferential attraction by measuring how γ changes with the correlation length, $\nu_o \lesssim 1$ and smaller κ are suggested to be favorable in Figs. 7 and 9. The expansion coefficients $\hat{\gamma}_n^{(k)}$ for $n = 1, 2, \dots$ and $k = 2, 3, \dots$ are not calculated in the present study, as shown in Fig. 3. Various integrals of damped-oscillating functions over a semi-infinite intervals are involved in the recurrence relations, as shown in Appendix B. We need to improve the procedure to shorten the computing time for the purpose of calculating the coefficients extensively. The deviation ratios shown in Fig. 9 almost vanish for a rigid disk irrespective of the values of ν_o . However, the ratio for a rigid disk may be definitely positive or negative for some parameter values of (ν_o, s_c) not yet examined. This point remains to be studied. Calculating the drag coefficient of a domain beyond the regime of the Gaussian model is another future work. We would have to consider the inhomogeneity of the correlation length and transport coefficients beyond the regime, judging from the 3D mixture in a similar situation [51]. Some clues may be obtained from studies on the static properties of the membrane containing domains[60, 61].

ACKNOWLEDGMENTS

A part of the work was financially supported by Keio Gakuji Shinko Shikin.

Appendix A: Some details

For $R > 1$, Eq. (2.44) gives

$$\left(\frac{\partial^2}{\partial R^2} + \frac{1}{R} \frac{\partial}{\partial R} - \frac{1}{R^2} \right) \tilde{\mu}_1^{(1)} = -\frac{hr_0^2}{ML} \Phi(R) \left(\tilde{v}_{r1}^{(1)}(r) - \frac{U}{2} \right). \quad (\text{A.1})$$

Equation (2.45) gives $e_r \cdot \nabla \mu^{(1)} = 0$ at $r = r_0$, and $\tilde{\mu}_1^{(1)}(r)$ tends to zero as $r \rightarrow \infty$. Using Eq. (2.29), we can rewrite the rhs of Eq. (A.1) as

$$-\frac{hr_0^2 U}{2\chi ML} \Phi(R) \left([\mathcal{L}\hat{A}](R) - \chi \right). \quad (\text{A.2})$$

Regarding Eq. (A.1) as an inhomogeneous linear equation with constant coefficients, we can solve it formally. Writing $\Omega(R)$ for Eq. (A.2) here, we have

$$\tilde{\mu}_1^{(1)}(r) = [\Delta_1^{-1}\Omega](R). \quad (\text{A.3})$$

As shown by Eq. (2.51), Δ_1^{-1} involves the kernel G , which is the same as given by Eq. (3.57) of Fujitani [43]. Substituting Eq. (A.3) into the rhs of Eq. (2.48) yields Eq. (2.50). When κ vanishes, Eq. (2.15) and (2.48) are reduced to Eq. (3.26) of Fujitani [43], whose $\mathcal{A}(\zeta)$ and $\kappa(\rho)$ should be respectively read as $A(\zeta)/(2\eta_3 r_0^2 U)$ and $\Phi(R)$ defined in the present study.

As mentioned in Sect. 2 B, we in general have Eq. (2.40) with $\mu^{(0)}$ being replaced by $\mu(\mathbf{r})$, and thus $(m - M\Delta)\varphi^{(1)} = \mu^{(1)}$. Equation (2.41) yields $e_r \cdot \nabla\varphi^{(1)} = 0$ at $r = r_0$, while $\varphi^{(1)}(r)$ tends to zero as $r \rightarrow \infty$. We thus have

$$\tilde{\varphi}_1^{(1)}(r) = -\frac{r_0^2}{M} \int_1^\infty dR' \frac{\Gamma(R, R')}{R} \tilde{\mu}_1^{(1)}(r_0 R'), \quad (\text{A.4})$$

where the kernel Γ is defined by Eq. (3.55) of Fujitani [43]. We need not know its full expression, and here use only

$$\Gamma(1, R) = \frac{R s_c \Phi(R) K_1(s_c^{-1})}{K_1'(s_c^{-1})}. \quad (\text{A.5})$$

The x -component of the drag force is given by the sum of Eqs. (3.29) and (3.30) of Fujitani [43]. Part of this sum is rewritten with the aid of its Eq. (3.31) and the statement below its Eq. (3.32). Thus, γ is found to be given by the sum of Eq. (2.18) and

$$\frac{2\pi h \tilde{\varphi}_1^{(1)}(1)}{U} \left(1 + \frac{K_0(s_c^{-1})}{s_c K_1(s_c^{-1})} \right). \quad (\text{A.6})$$

Using Eqs. (A.3) and (A.4), we can transform Eq. (A.6) into Eq. (2.55). In this transformation, it is helpful to rewrite $s_c K_1(s_c^{-1})$ and $K_1'(s_c^{-1})$ in terms of $K_0(s_c^{-1})$ and $K_2(s_c^{-1})$.

For description of the recurrence relations, we rewrite double integrals contained in each of $[\mathcal{LH}\Omega](R)$ and $[\mathcal{NH}\Omega](R)$, where Ω is a function. In each, when the integrand converges absolutely, the function is continuous at $R = 1$ and the order of the integrals can be exchanged to yield

$$[\mathcal{LH}\Omega](1) = \int_1^\infty dR R \Phi(R) \Omega(R) [\mathcal{L}\hat{A}_0^{(0)}](R) \quad (\text{A.7})$$

and

$$[\mathcal{NH}\Omega](1) = \int_1^\infty dR \Phi(R) \Omega(R) w(R), \quad (\text{A.8})$$

where

$$w(R) \equiv \int_0^\infty d\zeta \frac{J'_2(\zeta)J_1(\zeta R)}{1 + \nu_0 \zeta}. \quad (\text{A.9})$$

We also introduce

$$T_n^{(k)}(R) \equiv \Phi(R) \left[\Delta_1^{-1} \Phi \left(\mathcal{L} \hat{A}_n^{(k)} - \delta_{n0} \delta_{k0} \chi \right) \right] (R). \quad (\text{A.10})$$

We substitute Eqs. (3.1)-(3.3) into Eqs. (2.26), (2.32), and (2.35) with Eqs. (2.52), (3.11), and (3.12) being supplemented respectively. The results for $k = 1, 2, \dots$ are as follows. We have $\beta_0^{(k)} = 0$ and

$$\beta_n^{(k)} = \nu_0 \left(\alpha_{n-1}^{(k)} \left[\mathcal{N} \hat{A}_0^{(0)} \right] (1) + \beta_{n-1}^{(k)} g + \left[\mathcal{N} \mathcal{M} \hat{A}_{n-2}^{(k)} \right] (1) + \int_1^\infty dR T_{n-1}^{(k-1)}(R) w(R) \right) \quad (\text{A.11})$$

for $n = 1, 2, \dots$, where we stipulate $\hat{A}_{-1}^{(k)} = 0$. For $n = 0, 1, \dots$, we have

$$\alpha_n^{(k)} = -\frac{1}{\chi} \left\{ \beta_n^{(k)} \left[\mathcal{L} J_0 \right] (1) + \left[\mathcal{L} \mathcal{M} \hat{A}_{n-1}^{(k)} \right] (1) + \int_1^\infty dR R T_n^{(k-1)}(R) \left[\mathcal{L} \hat{A}_0^{(0)} \right] (R) \right\} \quad (\text{A.12})$$

$$\text{and } \hat{A}_n^{(k)} = \alpha_n^{(k)} \hat{A}_0^{(0)} + \beta_n^{(k)} J_0 + \mathcal{M} \hat{A}_{n-1}^{(k)} + \left[S T_n^{(k-1)} \right] (\zeta), \quad (\text{A.13})$$

where the operator S is so defined that

$$\left[S T_n^{(k-1)} \right] (\zeta) \equiv \frac{1}{\zeta} \int_1^\infty dR J_1(\zeta R) T_n^{(k-1)}(R) \quad (\text{A.14})$$

holds. For convenience of numerical calculations, we utilize Eq. (A.13) in Eq. (3.5) to obtain

$$\hat{\gamma}_n^{(k)} = \alpha_n^{(k)} + 2\beta_n^{(k)} + \Theta \mathcal{M} \hat{A}_{n-1}^{(k)} + \int_1^\infty dR R T_n^{(k-1)}(R) \quad (\text{A.15})$$

for $n = 0, 1, \dots$. Here, we note that $\Theta S T_n^{(k-1)}$ vanishes because of the statement at the end of Appendix C of Fujitani [43].

The drag coefficient for $\kappa = 0$ up to the order of λ^2 was studied in Fujitani [43], whose Eq. (3.25) should have had $\mathbf{v}^{(1)} - U \mathbf{e}_x$ instead of $\mathbf{v}^{(1)}$ [62]. The corrected equation generates Eq. (A.1) of the present study. The missed term, $-U \mathbf{e}_x$, is found to generate the term involving χ in Eq. (A.10), which is contained in the first and fourth terms on the rhs of Eq. (A.15) for $n = 0$ and $k = 1$. In particular, χ in the fourth term makes $\hat{\gamma}_0^{(1)}$ positive; this positivity is shown in Fig. 8(a). The factor d in Eq. (3.59) of Fujitani [43] was erroneously found to be negative because of the missed term. This factor should equal $\hat{\gamma}_0^{(1)}$ in the present study; it is positive and is roughly proportional to s_c^4 for small s_c , as shown in Fig. 4(a).

Appendix B: Numerical procedure

In the recurrence relations, we encounter various integrands each of which contains a function generated after the operation of \mathcal{M} . For example, $\mathcal{N}\mathcal{M}\hat{A}_{n-2}^{(0)}$ and $\mathcal{L}\mathcal{M}\hat{A}_{n-1}^{(0)}$ in Eqs. (3.6) and (3.7) contain this kind of integrands. It is helpful in calculating the integration over a semi-infinite interval numerically to find how the integrand behaves for its large variable. As described in Appendix C of Tani and Fujitani [26], part of $\mathcal{M}J_0$ has a peculiar logarithmic dependence for its large variable, although $[\mathcal{N}\mathcal{M}J_0](R)$ is continuous at $R = 1$. Let us define $\hat{B}_n^{(0)}$ as $\hat{A}_n^{(0)} - \beta_n^{(0)}J_0$ to calculate $\mathcal{M}J_0$ separately. We find that $[\mathcal{M}\hat{B}_n^{(0)}](\xi)$ is asymptotically proportional to

$$\frac{1}{\xi \sqrt{\xi}} \cos(\xi + \delta) \quad (\text{B.1})$$

as ξ becomes large. We can fix the constant of proportionality and the phase shift δ from the numerical calculation of the function for relatively small ξ . The phase shift is close to $\pi/4$, as suggested in Fujitani [63].

We can replace $\mathcal{M}\hat{A}_m^{(0)}$ by $\beta_m^{(0)}\mathcal{M}J_0 + \mathcal{M}\hat{B}_m^{(0)}$ in Eqs. (3.6) and (3.7). The term $\Theta\mathcal{M}\hat{A}_{n-1}^{(0)}$ in Eq. (3.10) is rewritten as $\beta_{n-1}\Theta\mathcal{M}J_0 + \Theta\mathcal{M}\hat{B}_{n-1}^{(0)}$. To calculate $\Theta\mathcal{M}\hat{B}_{n-1}^{(0)}$ numerically, we can utilize Eq. (C3) of Ref, Tani and Fujitani [26], as suggested below this equation. It is thus convenient to use

$$\mathcal{M}\hat{B}_n^{(0)} = \alpha_n^{(0)}\mathcal{M}\hat{A}_0^{(0)} + \beta_{n-1}^{(0)}[\mathcal{M}\mathcal{M}J_0] + [\mathcal{M}\mathcal{M}\hat{B}_{n-1}^{(0)}], \quad (\text{B.2})$$

instead of Eq. (3.8), in the recursion relations for $\lambda = 0$. The last term above also asymptotically proportional to Eq. (B.1) for large variable.

The above procedure is also available in the recursion relations for $\lambda \neq 0$, *i.e.*, Eqs. (A.11)-(A.13) and (A.15). The term $\mathcal{L}\hat{A}_n^{(0)}$ in Eq. (A.10) for $k = 0$ is calculated by means of Eq. (3.8), whose last term can be rewritten as $\beta_{n-1}^{(0)}[\mathcal{M}J_0] + [\mathcal{M}\hat{B}_{n-1}^{(0)}]$. As ξ increases, $[\mathcal{M}ST_n^{(1)}](\xi)$ is asymptotically proportional to Eq. (B.1) with δ being close to $3\pi/4$.

Appendix C: Transport coefficients

By considering the equilibrium fluctuation of a near-critical fluid, one finds that the transport coefficient on large length scales should be affected by the convection due to long-lived correlated

clusters smaller than the correlation length [31]. The Onsager coefficient L appearing in Eq. (2.44) should be regarded as already coarse-grained up to the correlation length, denoted by ξ_c . We can find how L depends on ξ_c by applying the mode-coupling theory, where the nonlinear dynamics is projected on the linear dynamics with the nonlinear terms being considered up to the second order [31, 64–66]. The calculation procedure used in the application of the mode-coupling theory for the model H is here available, except that the Oseen tensor should be modified to fit the fluid membrane immersed in a 3D fluid, as discussed in Fujitani [35]. The experimental results in Honerkamp-Smith *et al.* [34] is well explained by the theoretical results derived in Inaura and Fujitani [32], which are below improved in some points.

The fluid membrane considered here is the same as considered in Sect. 2 B, except that it has no circular liquid domain and that it has the critical composition. The order parameter ψ is defined as the deviation of φ from its critical value. From the first term of Eq. (2.36), the free-energy functional corresponding with the grand potential is found to be the integral of $(m\psi^2 + M|\nabla\psi|^2)/2$ over the membrane. We assume the dependence of ψ on \mathbf{r} and the time t to study its local fluctuation, write $C(\mathbf{r}, t)$ for the equilibrium average of $\psi(\mathbf{r}, t)\psi(0, 0)$, and below consider its Fourier transform with respect to x and y -components of \mathbf{r} . The relaxation constant of the Fourier transform with the 2D wavenumber vector \mathbf{q} is given by the sum of the van Hove term involving the bare value of L , denoted by $L^{(b)}$, and

$$\frac{k_B T}{4\pi^2} \int d\mathbf{p} \frac{p^2 q^2 - (\mathbf{p} \cdot \mathbf{q})^2}{2\eta_3 |\mathbf{p} - \mathbf{q}| + \eta_0 |\mathbf{p} - \mathbf{q}|^2} \frac{1 + q^2 \xi_c^2}{1 + p^2 \xi_c^2}, \quad (\text{C.1})$$

where p and q respectively denote $|\mathbf{p}|$ and $|\mathbf{q}|$. The above is equivalent to Eq. (2.21) of Inaura and Fujitani [32]; the infra-red cutoff of the integration is put equal to be zero, as in the derivation of the Kawasaki function in the mode-coupling theory for the model H. The van Hove term is given by $ML^{(b)}q^2(q^2 + \xi_c^{-2})$, as mentioned in Inaura and Fujitani [32]. The Onsager coefficient L appearing in Eq. (2.44) is so defined that the sum of the two terms are equal to the van Hove term with $L^{(b)}$ being replaced by L . Thus, the quotient of Eq. (C.1) divided by $Mq^2(q^2 + \xi_c^{-2})$ equals $L - L^{(b)}$, where the microscopic value $L^{(b)}$ is expected to be much smaller than L . The interdiffusion coefficient, denoted by D , is defined as the quotient of the relaxation constant divided by q^2 .

In Eq. (C.1), we change the variable of the integration into $\mathbf{K} \equiv (\mathbf{q} - \mathbf{p})\xi_c$, and the integration

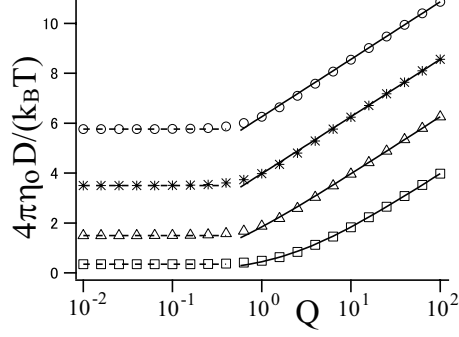


FIG. 10. Circles, asterisks, triangles, and squares represent Eq. (C.2) multiplied by $4\pi\eta_0/(k_B T)$ for $N = 3.2 \times 10^{-3}$, $\times 10^{-2}$, $\times 10^{-1}$, and $\times 10^0$, respectively. The solid curves from the top to the bottom represent the sum in the braces on the rhs of Eq. (C.5) for the values of N above, respectively. The dashed lines from the top to the bottom represent the second fraction on the rhs of Eq. (C.3) for the values of N , respectively.

with respect to its angular component of \mathbf{K} gives

$$D = \frac{k_B T (1 + Q^{-2})}{8\pi\eta_0} \int_0^\infty dK \frac{Q^2 + K^2 + 1 - \sqrt{(Q^2 + K^2 + 1)^2 - 4Q^2 K^2}}{K^2 (K + N)}, \quad (\text{C.2})$$

where we use $Q \equiv q\xi_c$ and $N \equiv 2\eta_3\xi_c/\eta_0 = s_c/\nu_0$. When Q is much smaller than unity, D is approximately equal to ML/ξ_c^2 , while Eq. (C.2) leads to

$$D \approx \frac{k_B T}{4\pi\eta_0} \int_0^\infty dK \frac{1}{(K + N)(K^2 + 1)} = \frac{k_B T}{4\pi\eta_0} \frac{\pi N - 2 \ln N}{2(1 + N^2)}, \quad (\text{C.3})$$

which is equivalent to Eq. (3.2) of Inaura and Fujitani [32]. When Q is much larger than unity, Eq. (C.2) leads to

$$D \approx \frac{k_B T}{4\pi\eta_0} \left[\int_0^Q dK \frac{1}{K + N} + \int_Q^\infty dK \frac{Q^2}{K^2 (K + N)} \right] \quad (\text{C.4})$$

$$= \frac{k_B T}{4\pi\eta_0} \left[\ln \left(1 + \frac{Q}{N} \right) + \frac{Q}{N} - \frac{Q^2}{N^2} \ln \left(1 + \frac{N}{Q} \right) \right], \quad (\text{C.5})$$

which is newly derived here. Figure 10 shows that these approximations work well. For $N \ll Q$, the sum in the braces on the rhs of Eq. (C.5) is approximately equal to $(1/2) + \ln(Q/N)$.

We below calculate the dependence of η_0 on ξ_c . Writing $\eta_0^{(b)}$ for its bare value, we apply the mode-coupling theory to find that $\eta_0 - \eta_0^{(b)}$ is given by [31]

$$\frac{M^2}{k_B T} \int_0^\infty dt \int d\mathbf{r} \left[\frac{\partial^2 C}{\partial x^2} \frac{\partial^2 C}{\partial y^2} + \left(\frac{\partial^2 C}{\partial x \partial y} \right)^2 \right], \quad (\text{C.6})$$

where C implies $C(\mathbf{r}, t)$ and the integral with respect to \mathbf{r} should be taken over the length scales from the microscopic scale (denoted by l_0) to ξ_c . The above can be rewritten as

$$\frac{k_B T}{8\pi} \int_{1/\xi_c}^{1/l_0} dq \frac{q^5}{(q^2 + \xi_c^{-2})^2} \int_0^\infty dt e^{-2Dq^2 t}. \quad (\text{C.7})$$

When N is much smaller than unity, *i.e.*, when ξ_c is much smaller than $\eta_o/(2\eta_3)$, we use the approximation for D mentioned at the end of the preceding paragraph to obtain

$$\eta_o \approx \eta_o^{(b)} \left[1 + \int_1^{\xi_c/l_0} dQ \frac{1}{2Q + 4Q \ln(Q/N)} \right] \quad (\text{C.8})$$

$$\propto \left[1 + \frac{\ln(\xi_c/l_0)}{(1/2) - \ln N} \right]^{1/4} \approx \left[\ln \frac{\eta_o^{(b)}}{2\eta_3 \xi_c} \right]^{-1/4}, \quad (\text{C.9})$$

which represents weak dependence of η_o on ξ_c . We can calculate the integral of Eq. (C.8) numerically by using the rhs of Eq. (C.5) even when $N \ll Q$ cannot be assumed in the integrand. According to the results not shown here, η_o triples at the most as ξ_c changes from 1 to 100 nm for practically possible material constants. Thus, for the parameter values considered in the text, the dependence of η on ξ_c can be neglected. In passing, the corresponding calculation in the model H for a 3D mixture gives the shear viscosity proportional to the correlation length to the power $8/(15\pi^2)$ [31, 67, 68]. The power is given by $(d-2)/3$ for an isolated d -dimensional fluid, when d is the real-valued dimension close to and larger than two [67, 68].

-
- [1] W. Sutherland, *Phil. Mag.* **9**, 781 (1905).
 - [2] A. Einstein, *Ann. Phys. (Leipzig)* **322**, 549 (1905).
 - [3] X. Bian, C. Kim, and G. E. Karniadakis, *Soft Matter* **12**, 6331 (2016).
 - [4] T. A. Waigh, *Rep. Prog. Phys.* **68**, 685 (2005).
 - [5] P. Domínguez-García, F. Cardinaux, E. Bertseva, L. Forró, F. Scheffold, and S. Jeney, *Phys. Rev. E* **90**, 060301 (2014).
 - [6] R. Glazier and K. Salaita, *Biophys. Biochim. Acta* **1859**, 1465 (2017).
 - [7] F. Ortega, H. Ritacco, and R. G. Rubio, *Curr. Opin. Colloid Interface Sci.* **15**, 237 (2010).
 - [8] T. Franosch, M. Grimm, M. Belushkin, F. M. Mor, G. Foffi, L. Forró, and S. Jeney, *Nature* **478**, 85 (2011).
 - [9] M. Grimm, T. Franosch, and S. Jeney, *Phys. Rev. E* **86**, 021912 (2012).
 - [10] S. J. Singer and G. L. Nicolson, *Science* **175**, 720 (1972).

- [11] S. Komura and D. Andelman, *Adv. Colloid Interface Sci.* **208**, 34 (2014).
- [12] P. G. Saffman and M. Delbrück, *Proc. Natl. Acad. Sci. U. S. A.* **72**, 3111 (1975).
- [13] P. G. Saffman, *J. Fluid Mech.* **73**, 593 (1976).
- [14] B. D. Hughes, B. A. Pailthorpe, and L. R. White, *J. Fluid Mech.* **110**, 349 (1981).
- [15] K. Simons and E. Ikonen, *Nature* **387**, 569 (1997).
- [16] M. Leslie, *Science* **334**, 1046 (2011).
- [17] C. Dietrich, L. A. Bagatolli, Z. N. Volovyk, N. L. Thompson, K. J. M. Levi, and E. Gratton, *Biophys. J.* **80**, 1417 (2001).
- [18] S. L. Veatch and S. L. Keller, *Phys. Rev. Lett.* **89**, 268101 (2002).
- [19] S. L. Veatch and S. L. Keller, *Biophys. J.* **85**, 4428 (2003).
- [20] S. L. Veatch and S. L. Keller, *Phys. Rev. Lett.* **94**, 148101 (2005).
- [21] S. L. Veatch, O. Soubias, S. L. Keller, and K. Gawrisch, *Proc. Natl. Acad. Sci. U. S. A.* **104**, 17650 (2007).
- [22] R. D. Koker, *The Program in Biophysics*, Ph.D. thesis, Stanford University (1996).
- [23] P. Cicuta, S. L. Keller, and S. L. Veatch, *J. Phys. Chem.* **111**, 3328 (2007).
- [24] S. Aliaskarisohi, P. Tierno, P. Dhar, Z. Khattari, M. Blaszczyński, and T. M. Fischer, *J. Fluid Mech.* **654**, 417 (2010).
- [25] Y. Fujitani, *J. Phys. Soc. Jpn.* **82**, 084403 (2013).
- [26] H. Tani and Y. Fujitani, *J. Fluid Mech.* **836**, 910 (2018).
- [27] A. R. Honerkamp-Smith, P. Cicuta, M. D. Collins, S. L. Veatch, M. den Nijs, M. Schick, and S. L. Keller, *Biophys. J.* **95**, 236 (2008).
- [28] S. L. Veatch, P. Cicuta, P. Sengupta, A. R. Honerkamp-Smith, D. Holowka, and B. Baird, *ACS Chem. Biol.* **3**, 287 (2008).
- [29] A. R. Honerkamp-Smith, S. L. Veatch, and S. L. Keller, *Biochim. Biophys. Acta* **1788**, 53 (2009).
- [30] P. C. Hohenberg and B. I. Halperin, *Rev. Mod. Phys.* **49**, 435 (1977).
- [31] A. Onuki, *Phase Transition Dynamics* (Cambridge University Press, 2002) Chap. 6.
- [32] K. Inaura and Y. Fujitani, *J. Phys. Soc. Jpn.* **77**, 114603 (2008).
- [33] M. Haataja, *Phys. Rev. E* **80**, 020902 (2009).
- [34] A. R. Honerkamp-Smith, B. B. Machta, and S. L. Keller, *Phys. Rev. Lett.* **108**, 265702 (2012).
- [35] Y. Fujitani, *J. Phys. Soc. Jpn.* **82**, 014601 (2013).
- [36] Y. Tserkovnyak and D. R. Nelson, *Proc. Natl. Acad. Sci. U. S. A.* **103**, 15002 (2006).

- [37] V. Démery and D. S. Dean, Phys. Rev. Lett. **104**, 080601 (2010).
- [38] B. A. Camley and F. L. H. Brown, Phys. Rev. E **85**, 061921 (2012).
- [39] B. A. Camley and F. L. H. Brown, J. Chem Phys. **141**, 075103 (2014).
- [40] R. Okamoto, Y. Fujitani, and S. Komura, J. Phys. Soc. Jpn. **82**, 084003 (2013).
- [41] A. Furukawa, A. Gambassi, S. Dietrich, and H. Tanaka, Phys. Rev. Lett. **111**, 055701 (2013).
- [42] S. Yabunaka, R. Okamoto, and A. Onuki, Soft Matter **11**, 5738 (2015).
- [43] Y. Fujitani, J. Phys. Soc. Jpn. **82**, 124601 (2013), [erratum] **83**, 088001 (2014).
- [44] We rewrite $\tilde{p}_1^{(1)}$, contained in Eq. (2.17), by using the Fourier transform of the θ -component with the order of ε extracted from the first equation of Eq. (2.2).
- [45] Equation (2.18) can be derived from Eqs. (2.24), (2.41) and (3.13) of Fujitani [25].
- [46] The integral denoted by χ is referred to as $\chi(1)$ in Fujitani [43] and as Y_0 in Tani and Fujitani [26].
- [47] Numerical procedure of calculating g is described in Sect. 4.2 of Tani and Fujitani [26].
- [48] Y. Fujitani, J. Phys. Soc. Jpn. **83**, 024401 (2014), [erratum] **83**, 108001 (2014).
- [49] J. W. Cahn, J. Chem. Phys. **66**, 3667 (1976).
- [50] H. W. Diehl and H. K. Janssen, Phys. Rev. A **45**, 7145 (1992).
- [51] Y. Fujitani, J. Phys. Soc. Jpn. **86**, 044602 (2017).
- [52] Y. Fujitani, J. Phys. Soc. Jpn. **83**, 084401 (2014).
- [53] Y. Fujitani, J. Phys. Soc. Jpn. **85**, 044401 (2016).
- [54] A. J. Liu and M. E. Fisher, Phys. Rev. A **40**, 7202 (1989).
- [55] B. S. Carey, L. E. Scriven, and H. T. Davis, AIChE J. **26**, 705 (1980).
- [56] P. M. W. Cornelisse, C. J. Peters, and J. de Swaan Arons, Fluid Phase Equilib. **117**, 312 (1996).
- [57] J. B. A. F. Smeulders, C. Blom, and J. Mellema, Phys. Rev. A **42**, 3483 (1990).
- [58] Y. Fujitani, J. Phys. Soc. Jpn. **80**, 074609 (2011).
- [59] C. Peskin, Acta Numer. **11**, 479 (2002).
- [60] B. B. Machta, S. L. Veatch, and J. P. Sethna, Phys. Rev. Lett. **109**, 138101 (2012).
- [61] P. Nowakowski, A. Maciolek, and S. Dietrich, J. Phys. A: Math. Theor. **49**, 485001 (2016).
- [62] Accordingly, $\Lambda(\rho)$ should have been replaced by $\Lambda(\rho) - \chi(1)\kappa(\rho)$ in Fujitani [43].
- [63] Y. Fujitani, J. Phys. Soc. Jpn. **81**, 084601 (2012).
- [64] H. Mori, Prog. Theor. Phys. **30**, 423 (1965).
- [65] K. Kawasaki, Ann. Phys. (N. Y.) **61**, 1 (1970).
- [66] R. Zwanzig, *Nonequilibrium Statistical Mechanics* (Oxford University Press, 2001) sect. 9.

- [67] T. Ohta, Prog. Theor. Phys. **54**, 1566 (1975).
- [68] T. Ohta and K. Kawasaki, Prog. Theor. Phys. **55**, 1384 (1976).